Composites Part B 171 (2019) 154–165

Contents lists available at ScienceDirect

Composites Part B

journal homepage: www.elsevier.com/locate/compositesb

Enhancing flexural performance of ultra-high performance concrete by an optimized layered-structure concept

Y.Y.Y. Cao [1], P.P. Li [1], H.J.H. Brouwers, M. Sluijsmans, Q.L. Yu [*]

Department of the Built Environment, Eindhoven University of Technology, P.O. Box 513, 5600 MB, Eindhoven, the Netherlands

ARTICLE INFO

Keywords:
Layered cementitious composite
Ultra-high performance concrete
Fiber reinforcement
Flexural strength
Fracture

ABSTRACT

The study aims to improve the flexural behaviors of ultra-high performance fiber reinforced concrete (UHPFRC) by applying the concept of layered-structure. Deterministic criteria for layer cracking and debonding are proposed, formulas to predict the critical load at the first failure stage are developed, and effects of the layer E-modulus and thickness are assessed. Subsequently, double-layered UHPFRC beams are designed and tested under the three-point bending. Mechanical and interfacial properties of the beams are studied. Influences of the bottom layer thickness on the peak flexural load and the flexural energy are then investigated, which presents that a layer thickness ratio of 0.6 gives the optimum load carrying ability and beam flexural energy. The subsequent section discusses the effects of fiber re-arrangement on the flexural performances, revealing that the designed double-layered UHPFRC beam is able to withstand higher flexural load and energy than its single-layered counterpart with the same total fiber content. Moreover, it is exhibited that the peak flexural load is dependent on the fibers in the bottom layer while the flexural energy enhancement is related to fibers in both layers. The layered UHPFRC beam composed of a 40 mm-thick top layer with 0.6% steel fibers and a 60 mm-thick bottom layer with 1.6% fibers is an optimal choice leading to the superior peak flexural load and energy.

1. Introduction

Ultra-high performance fiber reinforced concrete (UHPFRC) is a construction material with superior mechanical and material properties [1–5]. However, the high production cost of UHPFRC limits its widespread utilization [5–7]. To broaden the application, achieving lower material costs of UHPFRC is an important issue. Replacing fine particles with cheaper coarse aggregates could be one of the solutions. Typically, coarse aggregates are eliminated from traditional UHPFRC to enhance its homogeneity and thereafter its strength. Despite that, current studies confirm the potential of incorporating coarse aggregates in UHPFRC. Studies show that UHPFRC with an appropriate content of coarse aggregates possess advantages on respects such as binder material saving, shrinkage control and impact resistance [5,8,9], and the strength loss can be limited by properly packing the granular constituents [8,10].

Besides the binder, another dominant factor in UHPFRC production is the cost of steel fibers [11,12], which stresses the necessity of using steel fibers more efficiently. Compared to the traditional reinforcing rebar, fiber reinforcement possesses a superior ability in controlling crack propagation and preventing abrupt failure [13,14], making it a common reinforcement employed in UHPFRC [15]. The application of steel fibers contributes significantly to the enhancement of UHPFRC tensile properties [15,16], and a strong dependency of the tensile strength on the fiber content is exhibited [17,18]. Nevertheless, previous studies suggest that steel fibers have less significant effects on improving the compressive strength of UHPFRC compared with that on the tensile strength [18–20]. As a consequence, it is uneconomical to distribute steel fibers in the whole volume of UHPFRC for many applications where the structure is partially in tension and partially in compression [13], e.g. bending beams and specimens under impact [21,22]. We can take the bending beam as an example. When a beam works under service situations, half of it is in tension and the other half in compression [22]; the fibers in the tensile zones could effectively improve the flexural strength of the beam after cracking occurs while those in the compressive zone have smaller contributions [23].

To generate a more efficient fiber utilization, optimization is required to selectively distribute the fibers in UHPFRC where their advantages can be fully exploited. An innovative approach is designing

* Corresponding author.
E-mail address: q.yu@bwk.tue.nl (Q.L. Yu).
[1] Equivalent first authors.

https://doi.org/10.1016/j.compositesb.2019.04.021
Received 5 March 2019; Received in revised form 4 April 2019; Accepted 22 April 2019
Available online 25 April 2019

layered UHPFRC with different fiber contents at specific depths. Cyclic loading and impact studies on normal concrete have confirmed the benefits of applying layered-structure to cementitious materials [24–26]. From these evidences, it is reasonable to hypothesize that a layered UHPFRC with fibers purposefully reinforced in the targeted region would have superior mechanical properties and advanced fiber efficiency in comparison to the single-layered UHPFRC with the same amount of fibers distributed randomly in the whole structure.

Load carrying capacity and flexural energy are two important factors for assessing the performance of cementitious materials, and three-point bending test is often used for the evaluation [27–29]. Current researches on flexural properties mainly concentrate on single-layered concrete [30–32], while multi-layered cementitious composites are insufficiently studied. Among the limited researches, most of them addressed the combination of old and new concretes as layered repair systems [33–35]. Only several studies investigated the bending performances of multi-layered concrete of which all the layers are freshly cast. Liu et al. [13] assessed the flexural strength of double-layered concrete beams (compressive strength smaller than 30 MPa), and claimed their potential applications in real construction. Shen et al. [22] studied the flexural behavior of a four-layered concrete beam with PVA fibers gradually distributed; their results show that the layered beam has a 50% higher flexural strength compared to its single-layered counterpart. It should be noted that the design of these layered cementitious composites is empirical, e.g. the thickness of the layer is randomly chosen and the influences of the layer thickness are not considered. Xu et al. [36] and Hou et al. [37] presented theoretical and experimental investigations on steel-bar reinforced concrete with an ultra-high flexural energy concrete (UHTCC) layer, in which effects of the reinforcement ratio and the layer thickness were discussed. It showed that the interface cracking and ultimate bonding strengths are related to the reinforcement ratio and UHTCC layer thickness. Furthermore, an theoretical model developed by Zhang et al. [38,39] was used for analyzing the flexural behaviors of engineered cementitious composites (ECC) with two layers. Their model and tests confirm that the ECC layer thickness is an important design parameter, and that the beam flexural strength increases non-linearly with the ECC thickness. Nonetheless, the above analytical researches are based on constitutive relationships of concretes (with reinforcing bars), i.e. stress–crack relations must be obtained in advance. Moreover, the model calculations require complex processes and massive programming efforts, which thus hinders its engineering applications. That being the case, proposing theoretical models which are simple and ready to be applied to layered-structure design is still of urgent importance.

In this study, flexural performances of double-layered UHPFRC composites incorporating coarse aggregates are investigated theoretically and experimentally. In the theoretical section, critical cracking and debonding criteria of the layered beam at the first failure stage are proposed, formulas for predicting the critical load are developed, and influences of the layer thickness are analyzed. With the support of the theoretical analysis, double-layered UHPFRC composite beams are designed in the subsequent experimental section, in which the theoretical and experimental first cracking loads are also compared. Moreover, enhancements of the flexural performance due to the fiber rearrangement in the layered structure, the effects of the layer interface on the crack development, and the roles of steel fibers in individual layers are discussed in detail. Results from this study provide an important perspective for understanding the flexural behaviors of layered UHPFRC. Additionally, with the incorporation of coarse aggregates and the efficient utilization of steel fibers, the designed double-layered UHPFRC beam can bring great economic benefits and hence promotes the future technological application of layered UHPFRC in engineering constructions.

2. Theoretical analysis of the first failure stage

In this section, a double-layered UHPFRC beam subjected to three point bending is considered, as shown in Fig. 1. The total thickness and width of the beam are H and b, correspondingly. E_1, h_1 and A_1 are the E-modulus, layer thickness and cross-sectional area of the top layer; E_2, h_2 and A_2 are those of the bottom layer, respectively. h_0 is the height of the neutral axis. F_s is the shear force, which equals to half of the external load F according to the force equilibrium. M is the bending moment in the beam at point x, i.e. $M(x) = Fx/2$, and it reaches the maximum value $M_{max} = FL/4$ at $x = L/2$.

The failure process of the beam under bending can be divided into two stages: (1) a linear elastic stage until first cracking and (2) a following fictitious crack developing stage [39]. This section focuses on the stress distribution at the first failure stage, considering the fact that the first cracking load can be used as an indicator to evaluate the flexural capacity of UHPFRC [40,41], as well as the simplicity and practicality of the proposed formula to support the structure design. In addition, since stress-strain relations of materials are not required in the analysis (only basic mechanical properties, e.g. tensile strength and E-modulus, are necessary), formulas in this section can also be extended to general layered composite made of materials other than concrete.

2.1. Cracking criteria in the layered UHPFRC beam

Plane section assumption is applied in the analysis, i.e. the cross section of the double-layered UHPFRC beam is considered to remain plane [38]. The equilibrium of the forces is expressed by:

$$\int_{A_1} \sigma_1 dA_1 + \int_{A_2} \sigma_2 dA_2 = 0 \tag{1}$$

which can be transformed to:

$$E_1 \int_{A_1} y dA_1 + E_2 \int_{A_2} y dA_2 = 0 \tag{2}$$

where σ_1 and σ_2 are the normal stress in the top and bottom layers, correspondingly. Then the height of the neutral axis h_0 could be obtained as:

$$h_0 = \frac{H\left[1 - \beta^2(1 - 1/\alpha)\right]}{2[1 - \beta(1 - 1/\alpha)]} \tag{3}$$

where $\alpha = E_1/E_2$ is the layer E-modulus ratio, and $\beta = h_2/H$ is the layer thickness ratio. For a single-layered beam, i.e. $\alpha = 1$, $\beta = 0$ or 1, Eq. (3)

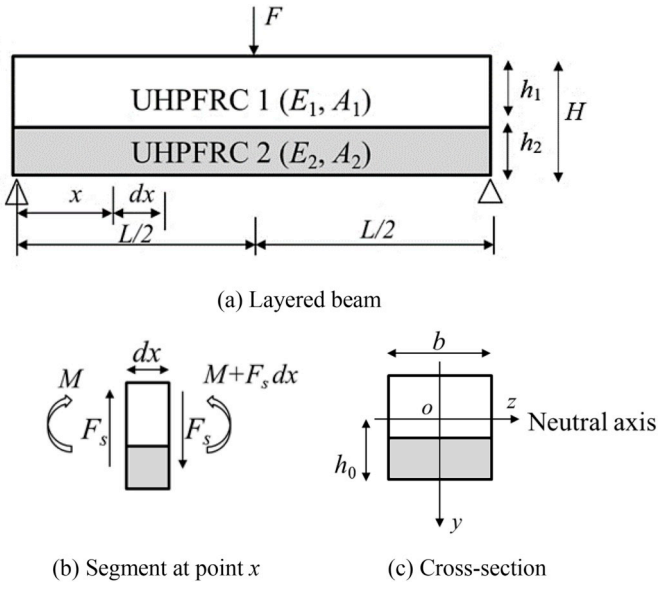

Fig. 1. Double-layered UHPFRC beam under bending.

reduces to $h_0 = H/2$.

Substituting $h_2 = h_0$ to Eq. (3) yields the critical layer thickness ratio β_c, in which case the entire bottom UHPFRC layer is exactly in tension and the entire top layer is exactly in compression:

$$\beta_c = \frac{\sqrt{\alpha}}{1+\sqrt{\alpha}} \tag{4}$$

When β_c $\beta \le 1$ is satisfied, h_2 is larger than h_0, i.e. the neutral axis is in the bottom layer. In this situation, the layer interface is within the range of the compression zone. Otherwise, the neutral axis is in the top layer, and the interface is under tension.

Based on the plane assumption of the beam section, the normal stress distributions in the two layers can be expressed as:

$$\text{Top layer: } \sigma_1(y) = \frac{My}{I_0},\ h_0 - H \le y < h_0 - h_2 \tag{5}$$

$$\text{Bottom layer: } \sigma_2(y) = \frac{My}{\alpha I_0},\ h_0 - h_2 \le y \le h_0 \tag{6}$$

I_0 is the inertia moment of the layered beam, which is a function of α and β:

$$I_0 = \frac{H^3 b}{12}\left[(1-\beta)^3 + \frac{\beta^3}{\alpha} + \frac{3\beta(1-\beta)}{\beta+\alpha(1-\beta)}\right] \tag{7}$$

For a given external load, the normal stress distribution along the layered beam section is plotted in Fig. 2a, where $\alpha = 0.8$, $\beta = 0.5$ are taken as an example. It can be seen from the figure that the normal stresses, i.e. compressive and tensile stresses, reach their maximum values at the top and bottom surfaces of the beam respectively, and a jump of the compressive stress is observed at the layer interface due to the change of the material properties of the two layers.

In general, crack initiates when the tensile stress in the UHPFRC beam exceeds its yield strength [42–44]. If the layer interface is within the range of the compression zone ($h_2 > h_0$), cracking always starts first from the lower position of the bottom layer (Fig. 2a). However, if the interface is in the tension zone ($h_0 > h_2$), the initial crack may appear first in the top layer. Assuming that the two layers reach their tensile strengths $\sigma_{t,i}$ ($i = 1, 2$) at the same time:

$$\sigma_1(y = h_0 - h_2) = \sigma_{t,1} \tag{8}$$

$$\sigma_2(y = h_0) = \sigma_{t,2} \tag{9}$$

the critical first cracking condition can be obtained:

$$\frac{\sigma_{t,1}}{\sigma_{t,2}} = \left(1 - \frac{h_2}{h_0}\right)\alpha = \frac{1 - 2\beta + \beta^2(1 - 1/\alpha)}{1 - \beta^2(1 - 1/\alpha)}\alpha = \gamma_c \tag{10}$$

Eq. (10) reveals that if the tensile strength of the top layer $\sigma_{t,1}$ is smaller than the value of $\gamma_c\ \sigma_{t,2}$, then, in theory, the first crack would occur in the top layer near the interface at $x = L/2$. In this case, the external load to evoke the first crack is:

$$F_{c,\text{top}} = \frac{4I_0\sigma_{t,1}}{Lh_0 - h_2} = \frac{2H^2 b\sigma_{t,1}[1-\beta(1-1/\alpha)]}{3L[1-2\beta+\beta^2(1-1/\alpha)]}\left[(1-\beta)^3 + \frac{\beta^3}{\alpha} + \frac{3\beta(1-\beta)}{\beta+\alpha(1-\beta)}\right] \tag{11}$$

Otherwise, the bottom layer cracks earlier and the corresponding critical load is:

$$F_{c,\text{bottom}} = \frac{4\alpha I_0\sigma_{t,2}}{Lh_0} = \frac{2\alpha H^2 b\sigma_{t,2}[1-\beta(1-1/\alpha)]}{3L[1-\beta^2(1-1/\alpha)]}\left[(1-\beta)^3 + \frac{\beta^3}{\alpha} + \frac{3\beta(1-\beta)}{\beta+\alpha(1-\beta)}\right] \tag{12}$$

In the specific case of a single-layered beam only composed of the UHPFRC 1 material (Fig. 1), i.e. $h_2 = 0$, $h_0 = H/2$, the critical load is expressed in Eq. (13), coinciding with the result obtained by substituting $\sigma_1\ (y = H/2) = \sigma_{t,1}$ in Eq. (5):

$$F_{c,\text{top},0} = \frac{8I_0\sigma_{t,1}}{LH} \tag{13}$$

Similarly, when $h_2 = H$, the beam is only composed of the UHPFRC 2 material. The critical load is Eq. (12) with $h_2 = H$ and $h_0 = H/2$, $\alpha = 1$, as given by:

$$F_{c,\text{bottom},0} = \frac{8I_0\sigma_{t,2}}{LH} \tag{14}$$

It is identical to Eq. (6) with $\sigma_2\ (y = H/2) = \sigma_{t,2}$ substituted. These agreements also confirm the correctness of the proposed equations.

Furthermore, it is worth to note that when the two layers have an equal E-modulus ($\alpha = 1$), the neutral axis is always at $h_0 = H/2$, and the value of I_0 as well as $F_{c,\text{bottom}}$ remain constant, i.e. changing the layer thickness h_2 has no influence under this circumstance. $F_{c,\text{top}}$ can be re-written as Eq. (15) when $\alpha = 1$ is substituted, the value of which increases with the increase of β, viz. when the crack initiates from the top layer ($0 < \beta < 0.5$ and $\sigma_{t,1} < \gamma_c\ \sigma_{t,2}$), the thicker the bottom layer the higher the first cracking load.

$$F_{c,\text{top}_{(\alpha=1)}} = \frac{2H^2 b\sigma_{t,1}}{3L(1-2\beta)} \tag{15}$$

2.2. Debonding criteria in the layered UHPFRC beam

The shear stress distributions in the two layers can also be obtained by the equilibrium of forces in x-axis direction (see Fig. 1):

$$\text{Top layer: } \int_{A1}\frac{My}{I_0}dA + \tau_1 \alpha b dx = \int_{A1}\frac{(M + F_s dx)y}{I_0}dA \tag{16}$$

$$\text{Bottom layer: } \int_{A2}\frac{My}{\alpha I_0}dA + \tau_2 b dx = \int_{A2}\frac{(M + F_s dx)y}{\alpha I_0}dA \tag{17}$$

The corresponding shear stresses in the two layers are given as:

$$\text{Top layer: } \tau_1(y) = \frac{F}{4I_0}\left[(H-h_0)^2 - y^2\right],\ h_0 - H \le y < h_0 - h_2 \tag{18}$$

$$\text{Bottom layer: } \tau_2(y) = \frac{F}{4\alpha I_0}\left(h_0^2 - y^2\right),\ h_0 - h_2 \le y \le h_0 \tag{19}$$

It is noted that the maximum shear stress along the beam depth is at the neutral axis $y = 0$ and the value is expressed as:

$$\tau_{max}(y = 0) = \frac{Fh_0^2}{4\alpha I_0} \tag{20}$$

Differing with the normal stresses, the shear stress changes continuously along the beam depth (see Fig. 2b) and the peak is at the location of the neutral axis, which is usually nearby the layer interface when the E-modulus of the two layer are not very distinct, e.g. $\alpha = 0.8$ in Fig. 2b.

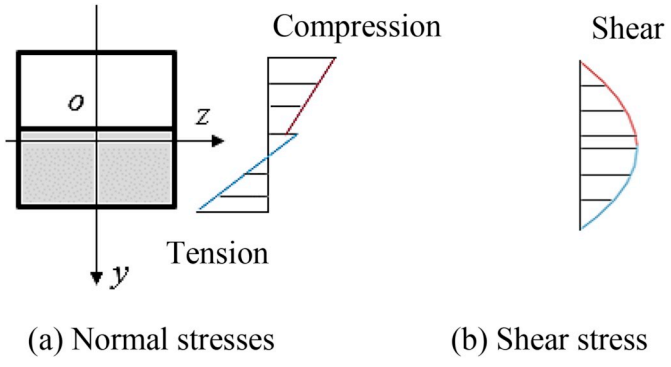

Fig. 2. Stress distribution along the layered beam in linear elastic stage.

This maximum shear stress can induce the possibility of layer debonding since the interface usually presents a weak part in the composite [45]. More specifically, debonding due to shear occurs when the interfacial shear stress reaches the bond strength σ_b:

$$\tau_1(y = h_0 - h_2) = \tau_2(y = h_0 - h_2) = \sigma_b \tag{21}$$

This leads to the critical debonding load provoked by shear:

$$F_{d,\text{shear}} = \frac{4\alpha I_0 \sigma_b}{h_2(2h_0 - h_2)} = \frac{\alpha H b \sigma_b [1 - \beta(1 - 1/\alpha)]}{3\beta(1 - \beta)} \left[(1 - \beta)^3 + \frac{\beta^3}{\alpha} + \frac{3\beta(1 - \beta)}{\beta + \alpha(1 - \beta)} \right] \tag{22}$$

On the other hand, when the layer interface is within the tension zone ($0 < h_2$ h_0), the tensile stress at the interface can also procure layer debonding when

$$\sigma_2(y = h_0 - h_2) = \sigma_b \tag{23}$$

Then the corresponding critical debonding load due to tension can be expressed as:

$$F_{d,\text{tension}} = \frac{4\alpha I_0 \sigma_b}{L(h_0 - h_2)} = \frac{2\alpha H^2 b \sigma_b [1 - \beta(1 - 1/\alpha)]}{3L[1 - 2\beta + \beta^2(1 - 1/\alpha)]} \left[(1 - \beta)^3 + \frac{\beta^3}{\alpha} + \frac{3\beta(1 - \beta)}{\beta + \alpha(1 - \beta)} \right] \tag{24}$$

When the critical debonding load is smaller than the critical cracking load, layer debonding occurs prior to layer cracking, which will strongly affect the effectiveness of the layered composite beam. To avoid early layer debonding, the following critical condition for the bond strength should be satisfied:

(1) If $h_2 \geq h_0$, the condition is $F_{\text{d,shear}} \geq F_{\text{c,bottom}}$:

$$\sigma_b \geq \frac{2\beta(1 - \beta)H}{[1 - \beta^2(1 - 1/\alpha)]L} \sigma_{t,2} \tag{25}$$

(2) If h_2 h_0, it turns to be Min ($F_{\text{d,shear}}$, $F_{\text{d,tension}}$) $\geq F_{\text{c,top}}$, for $\sigma_{t,1} < \gamma_c$ $\sigma_{t,2}$:

$$\sigma_b \geq \text{Max}\left(\frac{\sigma_{t,1}}{\alpha}, \frac{2\beta(1 - \beta)H}{[1 + \beta^2(1 - 1/\alpha) - 2\beta]L} \frac{\sigma_{t,1}}{\alpha} \right) \tag{26}$$

or Min ($F_{\text{d,shear}}$, $F_{\text{d,tension}}$) $\geq F_{\text{c,bottom}}$, for $\sigma_{t,1} \geq \gamma_c$ $\sigma_{t,2}$:

$$\sigma_b \geq \text{Max}\left(\frac{2\beta(1 - \beta)H}{[1 - \beta^2(1 - 1/\alpha)]L} \sigma_{t,2}, \frac{1 + \beta^2(1 - 1/\alpha) - 2\beta}{1 - \beta^2(1 - 1/\alpha)} \sigma_{t,2} \right) \tag{27}$$

2.3. Influences of α and β on stress distribution and critical load

Based on the above analysis, the critical load at the first stage of the failure process F_{critical} and the failure modes can be concluded as follows (also given in Table 1):

(1) For $h_2 = 0$ ($\beta = 0$): $F_{\text{critical}} = F_{\text{c,top,0}}$, the first failure stage ends with cracking of the beam (made of UHPFRC 1 material).
(2) For 0 < h2 < h0 (0 < β < βc) and σt,1 < γc σt, 2: Fcritical = Min (Fc,top, Fd,shear, Fd,tension), the first failure stage ends with top layer cracking or layer debonding. (3) For 0 < h2 < h0 (0 < β < βc) and σt,1 ≥ γc σt, 2: Fcritical = Min (Fc,bottom, Fd, shear, Fd,tension), the first failure stage ends with bottom layer cracking or layer debonding.
(4) For $h_0 \leq h_2$ H ($\beta_c \leq \beta < 1$): $F_{\text{critical}} = \text{Min}$ ($F_{\text{c,bottom}}$, $F_{\text{d,shear}}$), the first failure stage ends with bottom layer cracking or layer debonding due to shear.

Table 1
Critical load at first failure stage and the corresponding failure modes: F_{critical} = critical load, β = layer thickness ratio, β_c = critical layer thickness ratio, $\sigma_{t,i}$ ($i = 1, 2$) = layer tensile strength, γ_c = critical layer tensile strength ratio, $F_{\text{c, top}}$ = critical cracking load of the top layer, $F_{\text{c, bottom}}$ = critical cracking load of the bottom layer, $F_{\text{d,shear}}$ = critical debonding load by shear, $F_{\text{d,tension}}$ = critical debonding load by tension.

Conditions	F_{critical}	First stage failure modes
$\beta = 0$	$F_{\text{c,top,0}}$	(Single-layered) beam cracking
$0 < \beta < \beta_c$ and $\sigma_{t,1} < \gamma_c$ $\sigma_{t,2}$	Min ($F_{\text{c,top}}$, $F_{\text{d,shear}}$, $F_{\text{d, tension}}$)	Top layer cracking or layer debonding
$0 < \beta < \beta_c$ and $\sigma_{t,1} \geq \gamma_c$ $\sigma_{t,2}$	Min ($F_{\text{c,bottom}}$, $F_{\text{d,shear}}$, $F_{\text{d,tension}}$)	Bottom layer cracking or layer debonding
$\beta_c \leq \beta < 1$	Min ($F_{\text{c,bottom}}$, $F_{\text{d,shear}}$)	Bottom layer cracking or shear debonding
$\beta = 1$	$F_{\text{c,bottom,0}}$	(Single-layered) beam cracking

(5) For $h_2 = H$ ($\beta = 1$): $F_{\text{critical}} = F_{\text{c,bottom,0}}$, the first failure stage ends with cracking of the beam (made of UHPFRC 2 material).

The influences of α and β on h_0 and F_{critical} are plotted in Figs. 3 and 4, in which $H = 0.1$ m, $L = 0.4$ m, $\sigma_{t,1} = \sigma_b = 12$ MPa and $\sigma_{t,2} = 16$ MPa are taken as an example. Fig. 3 confirms that when the two layers have an identical E-modulus, i.e. $\alpha = 1$, the neutral axial is always at the middle of the beam depth regardless of the layer thickness, as expected. Consequently, the top half of the beam is always under compression while the bottom half is always in tension. On the other hand, h_0 changes with β when the two layers have different E-moduli. Moreover, if the top layer has a larger E-modulus, e.g. $\alpha = 1.2$, then h_0 is in the top half of the composite beam, indicating a larger tension region in the composite beam; otherwise, the compression region is more dominant (see Fig. 2a) and it extends with the decrease of α.

As analyzed, the damage modes at the first failure stage are related to β. For $\beta = 0.2$–1.0, the critical debonding load is much higher than the critical cracking load, and the first failure stage always ends with bottom layer cracking. In contrast, cases with $\beta = 0.1$ experience distinct damage modes (see Fig. 4): (1) for $\alpha = 0.8$ and 1.2, the initial crack appears in the top layer rather than in the bottom one since $\beta < \beta_c$ and $\sigma_{t,1} < \gamma_c$ $\sigma_{t,2}$; (2) for $\alpha = 0.6$, debonding due to tension occurs prior to cracking ($F_{\text{d, tension}} < F_{\text{c,top}}$), hence the failure is dominated by layer debonding; (3) for $\alpha = 1.0$, $F_{\text{d,tension}} = F_{\text{c,top}}$, i.e. debonding and cracking take place at the same time.

Furthermore, the relationship of F_{critical} and β is also depicted in Fig. 4. In the case of $\alpha = 1.0$, F_{critical} remains constant when β varies from 0.2 to 1.0, which is in line with the analysis in Section 2.1. In contrast,

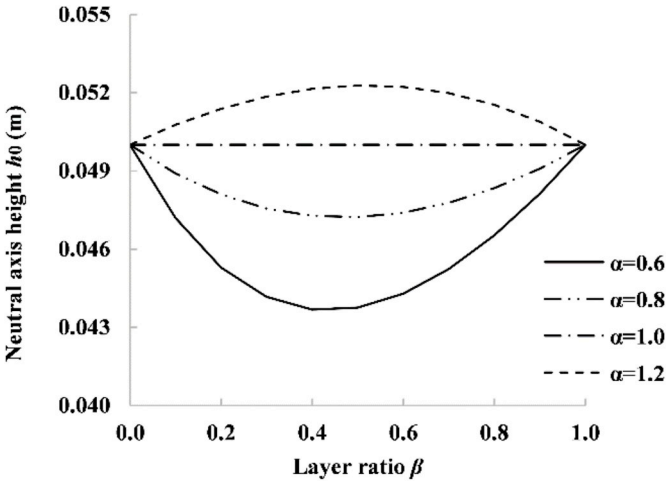

Fig. 3. Influences of the layer E-modulus ratio α and thickness ratio β on the neutral axial height h_0.

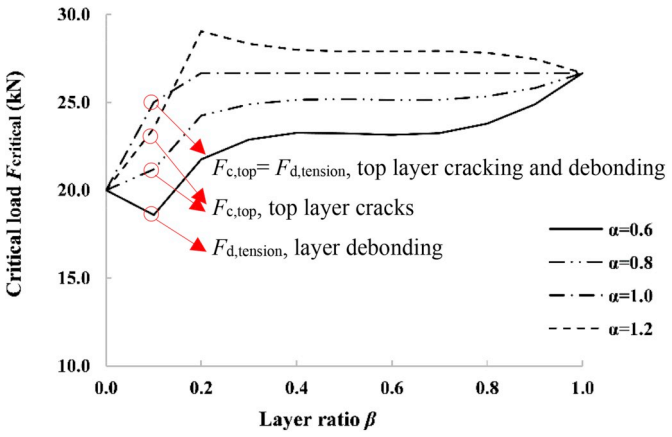

Fig. 4. Influences of the layer E-modulus ratio α and thickness ratio β on the critical load at the first stage of the failure process $F_{critical}$.

for $\alpha = 0.6$ and 0.8, $F_{critical}$ is improved when β increases from 0.2 to 1; the improvement is limited when β goes beyond 0.3, especially for $\alpha = 0.8$. In the case of $\alpha = 1.2$, a gradual decrease of the critical load is observed with the increase of β in the range of 0.2–1.0, indicating a negative effect of enhancing the bottom layer thickness on the cracking load despite its higher tensile strength.

3. Experimental program

3.1. Materials and mix design

The raw materials used for the UHPFRC are Portland Cement CEM I 52.5 R, densified micro-silica (Elkem Grade 920E D), limestone powder (CB2M, France), standard sand (based on DIN EN 196-1), basalt aggregates (produced in Gelderland, the Netherlands), tap water, a PCE based superplasticizer and smooth straight steel fiber. The chemical compositions and physical properties of powder are summarized in Table 2. The detailed properties of other raw materials can be found in Ref. [46].

The recipe of the UHPFRC matrix is based on the previous study [46], as presented in Table 3. The water to binder ratio remains a constant for all groups, i.e. w/b = 0.2. The coarse basalt aggregates applied have two size groups namely 2–5 mm and 5–8 mm, the fraction of which are calculated applying the Brouwers mix design method [47–50]. Smooth straight steel fibers (length = 13 mm, diameter = 0.2 mm, tensile strength = 2750 MPa) are utilized in the double-layered UHPFRC beams with different volume fractions in the individual layers. The amount of superplasticizer is adjusted with the fiber content [51] until a flowability around 560 mm is achieved [46] (measured with Abrams cone in accordance with EN 12350-8:2007 [52]).

Table 2
Physical and chemical properties of the powders: CEM = Portland cement, mS = micro-silica, LP = limestone powder.

Substituent (%)	CEM	mS	LP
Chemicals			
CaO	64.60	0.90	97.21
SiO_2	20.08	93.06	0.87
Al_2O_3	4.98	–	0.17
Fe_2O_3	3.24	2.06	0.13
K_2O	0.53	1.15	–
Na_2O	0.27	0.63	–
SO_3	3.13	1.28	0.11
MgO	1.98	0.70	1.17
TiO_2	0.30	–	0.01
MnO	0.10	0.07	0.01
Compounds			
C_3S	63.3	–	–
C_2S	9.8	–	–
C_3A	7.7	–	–
C_4AF	9.8	–	–
Specific density (g/cm^3)	3.15	2.32	2.71
BET surface area (m^2/kg)	1416	18432	1081

3.2. Design of double-layered UHPFRC composite beams

An identical recipe is applied for the matrixes in the individual UHPFRC layers while only the fiber and SP content vary (see Table 3). Consequently, the top and bottom layers of the UHPFRC composite beams have a similar compressive strength due to the insignificant effects of fiber content [18]. The similar matrixes of the two layers, on the one hand, can prevent interfacial debonding [53]; on the other hand, can benefit a direct comparison for investigating the effects of the layered structure.

Since the first cracking load can be used as an indicator to represent the maximum flexural capacity [40,41], thicknesses of the double-layered UHPFRC beams in this study are designed according to the theoretical first cracking load in Section 2. The relation between the critical load $F_{critical}$ and the layer thickness ratio β is referred. As suggested in Fig. 4 with $\alpha = 0.8$ and 1 (the layer E-modulus ratios of the designed beams are within this range), the enhancement of $F_{critical}$ is prominent when β increases from 0.1 to 0.3, whereas further thickening the bottom layer would not generate eminent improvement, viz. $\beta = 0.3$ is a threshold, below which the first cracking load still has a potential to increase. Thence, the thickness of the bottom layer h_2 should be larger than $0.3H$, otherwise $F_{critical}$ does not achieve its maximum. Additionally, considering the crack propagation at the second stage of the failure process and to investigate the effects of layer thickness on the composite flexural properties, three different layer thickness ratios are designed in the experimental section, namely $\beta = 0.4$, 0.6 and 0.8.

Detailed information about the designed double-layered UHPFRC beam is given in Table 4. The identification is defined as follows: U indicates the beam is a UHPFRC composite, the first number denotes the fiber volume fraction V_f in the top layer, and the following one in the brackets is the layer thickness in mm; the third and the fourth numbers are those for the bottom layer, correspondingly. For instance, U0.6(40)-1.6(60) is a double-layered UHPFRC beam of which the top layer has 0.6% fibers with a thickness of 40 mm, and the bottom layer contains 1.6% fibers and its thickness is 60 mm. Three single-layered UHPFRC beams (100 mm thick) with 0%, 1.2% and 2% fibers are included as reference groups, i.e. U0(100), U1.2(100) and U2(100), respectively. The groups are such designed that three influencing factors are addressed in the study as shown in Sections 4.2 to 4.4: five different values of β are analyzed in Section 4.2, which are typical and cover the main effective layer thickness range ($\beta > 0.3$); two different fiber rearrangements in the layered structure and one single-layered beam are compared in Section 4.3, the fiber content in the bottom layer varying from 1.2% to 2% as they can represent the most typical fiber amount in UHPFRC (further increasing the fiber content may lead to workability problems, especially for UHPFRC with coarse aggregates). It should be noted that these fiber volume fractions are just examples, and the concept and benefits of layered structure are also applicable to UHPFRC with higher fiber contents as long as the workability is satisfying. In Section 4.4, the effects of fiber in the individual layers on the flexural load and the energy are discussed, revealing the mechanisms of the fiber reinforcement.

3.3. Mixing and casting procedures

The following mixing procedure was adopted for the UHPFRC matrix: dry mixing for 2 min with all powders and sand; adding 75% of the water and mixing for 2 min; sequentially adding the remaining water with the superplasticizer and mixing for another 4 min, after which the steel fibers were added sequentially. Then the basalt aggregates were

Table 3
Recipes of the UHPC and the UHPFRC: CEM = Portland cement, mS = micro-silica, LP = limestone powder, S = sand, BA 2–5 = basalt aggregate with a diameter of 2–5 mm, BA 5–8 = basalt aggregate with a diameter of 5–8 mm, W = water, SP = superplasticizer, SF = steel fiber.

Materials	CEM (kg/m^3)	mS (kg/m^3)	LP (kg/m^3)	S (kg/m^3)	BA 2–5 (kg/m^3)	BA 5–8 (kg/m^3)	W[a] (kg/m^3)	SP[b] (kg/m^3)	SF (%)
Quantity	588	39.2	156.8	839.9	413.2	232.3	157	5.0	0
								7.0	0.6
								9.0	1.2
								14.0	1.6
								17.0	2.0

[a] Water from SP is included.
[b] The solid content is 35%.

Table 4
Layered UHPFRC composite beam: For the identification, U indicates UHPFRC; the first two numbers denote the fiber volume fraction and thickness of the top layer; and the last two numbers are those for the bottom layer.

Identification	Layer thickness (mm)		Fiber content (%)	
	Top layer	Bottom layer	Top layer	Bottom layer
U0(60)-2(40)	60	40	0	2
U0(40)-2(60)	40	60	0	2
U0(20)-2(80)	20	80	0	2
U0.6(40)-1.6(60)	40	60	0.6	1.6
U0(40)-1.2(60)	40	60	0	1.2
U0.6(40)-1.2(60)	40	60	0.6	1.2
U0(100)	100		0	
U1.2(100)	100		1.2	
U2(100)	100		2	

added to the mix and stirred for 3 min. The mixing procedure was conducted at room temperature (20 ± 1 °C).

100 × 100 × 500 mm^3 moulds were used for casting the beams. With regard to the double-layered UHPFRC beams, the bottom layer of the UHPFRC beam was cast in the mould with the designed thickness, and the top layer mixture was poured into the mould carefully 45 min later. This casting time interval is determined based on a preliminary study, considering both the experimental operability and the relation between the bond strength and the time interval. At the time of casting the top layer, the bottom layer was strong enough to support the top layer matrix, i.e. deformation of the layer interface was avoided; while the initial setting of the bottom layer matrix had not been reached [37,51], resulting in a strong interfacial bond. This casting method, on the one hand, induces to a sufficient layer bond strength; on the other hand, the existence of the layer interface can act as a source of micro-cracking, which consumes more fracture energy during the cracking process (this will be further explained in Section 4.3). Cubic moulds (100 × 100 × 100 mm^3) were used for the compressive, tensile and bond tests. The same casting method was applied for the double-layered cubes to test the interfacial bond strength. Cubes of single type UHPFRC mixtures (Table 3) were also cast to test the basic mechanical properties of the individual layers. The cast specimens were covered with plastic sheets for 24 h. Then they were demolded and cured in water for additional 27 days.

3.4. Testing methods

The compressive strengths of the UHPFRC samples were measured using a DIGIMAXX C-20 universal testing machine with a maximum load capacity of 4000 kN according to EN 12390-3 [54]. Splitting tensile tests based on EN 12390-6 [55] were conducted to obtain the tensile and interface bond strengths [56].

To investigate the flexural performances of the double-layered UHPFRC beams, three-point bending tests were conducted at the age of 28 days [39]. The span length was 400 mm [57]. The beams were not notched in this study because the notch would weaken the bottom layer and lead to difficulties in comparing fibers effects on individual layers. Displacement control under a rate of 0.2 mm/min was used in the test [58]. The applied load was measured by the Instron 5985 testing machine and the mid-point deflections were measured with two linear variable differential transducers (LVDTs) [36,59].

4. Experimental results and discussion

4.1. Mechanical and interfacial properties

The compressive and splitting tensile strengths of the individual UHPFRC layers with V_f = 0%, 0.6%, 1.2%, 1.6% and 2% are given in Fig. 5. As expected, the splitting tensile strength increases significantly with the increasing fiber content. For instance, a 97.3% enhancement of the 28d splitting tensile strength is observed for the UHPFRC incorporating 2% fibers compared to that of the mixture without fibers. In contrast, the improvement of the compressive strength is limited, i.e. the 28d compressive strengths for the matrixes are within the range of 140–153 MPa.

Fig. 6 shows the layer interface in the cube for the bond test, in which the combination of V_f = 2% and 0% layers is given as an example. The layer interface is rather invisible, but can be observed with careful look (see Fig. 6a). Cohesion failure occurs in the bond spitting test and the failure surface is shown in Fig. 6b and c. Fig. 7 plots the bond strengths of the tested group. The maximum bond strength is obtained for the interface between the V_f = 0.6% and 1.6% layers, which is around 9.28 MPa.

After acquiring the basic properties, the flexural performances of the designed double-layered UHPFRC composite beams are investigated. During the three-point bending tests, no debonding is observed thanks to the excellent interfacial bond strength resulted from the efficient casting method. The tested beams were cut with a saw after the bending experiments to check the layer interface. Photos of half of the tested U0 (40)-2(60) beam are given in Fig. 8 as an example. A straight layer interface is observed in the outer surface of the beam (Fig. 8a), and it can

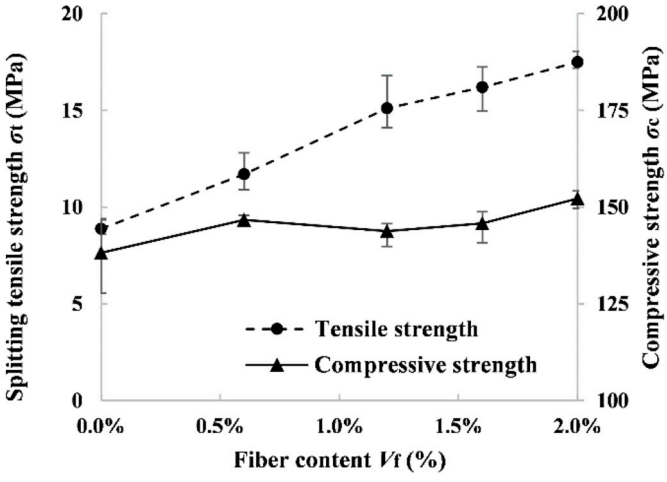

Fig. 5. Compressive and tensile strengths of mixtures in individual layers.

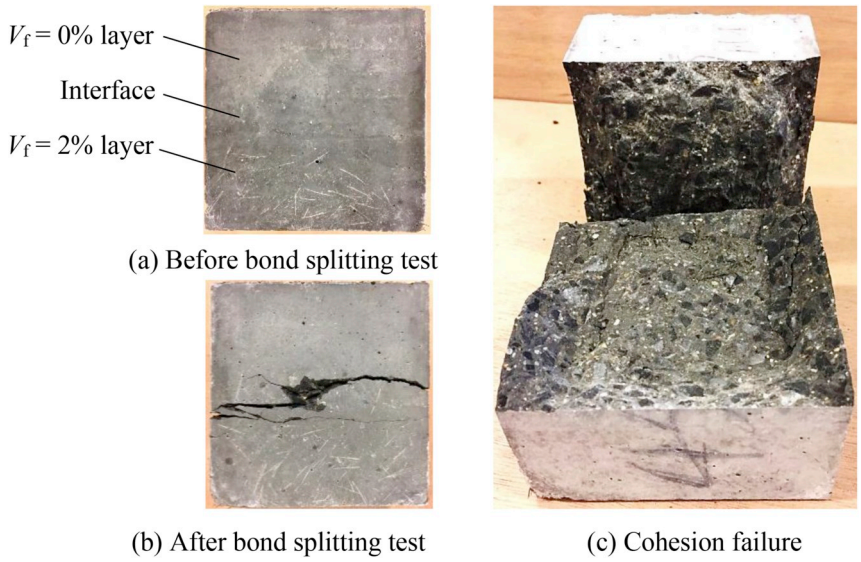

Fig. 6. Bond interface and failure surface.

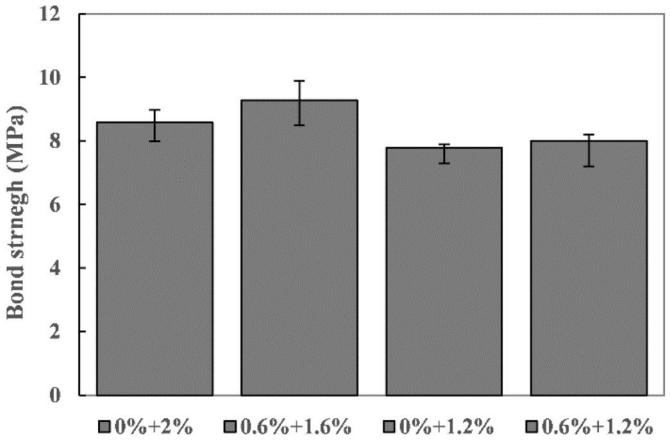

Fig. 7. Bond strengths of the layer interface.

also be observed in the cutting surface (Fig. 8b) where the bright dots in the bottom layer are the cross sections of the fibers. As presented in the figures, the layer interface is straight, confirming that the deformation of the bottom layer is very limited; and the material transition of the two layers is smooth, attributing to the strong bond of the layered beam. Additionally, it should be noted that since the top layer was cast before the bottom layer had reached the initial setting, the fresh mixture of the top layer should be poured slowly and evenly on the bottom layer with care to avoid large deformation of the bottom layer. Furthermore, in this study the top layer was cast on the bottom layer without special treatment of the contact surface, i.e. the strong interfacial bond is achieved by controlling the casting time interval rather than using any surface treatments. Nevertheless, when using the layered structure for commercial UHPFRC, surface treatment such as roughening the contact surface in fresh state would also be a solution to further enhance the bond strength [60], especially in the situation where the time interval is difficult to be controlled.

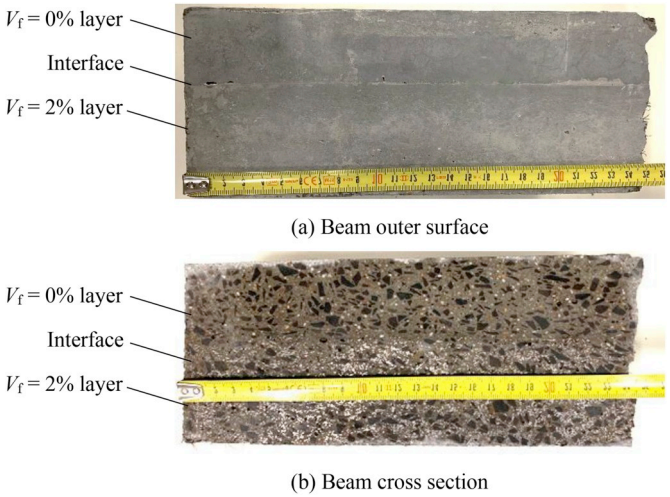

Fig. 8. Bond interface of the tested U0(40)-2(60) beam.

4.2. Effects of layer thickness

Fig. 9 plots the flexural performances of the double-layered UHPFRC beams with different layer thicknesses, of which the bottom layers contain 2% steel fibers and the top layers are without fibers. The performances of the single-layered beams with 0% and 2% fibers are also illustrated in the figure, i.e. U0(100) and U2(100). Distinct failure modes are observed for the beams with and without the fiber-reinforced layer, i.e. the plain single-layered beam experienced a catastrophic and brittle failure as opposed to the gradual failure of the composite beams reinforced with the 2% fiber layer. In addition, the first crack always

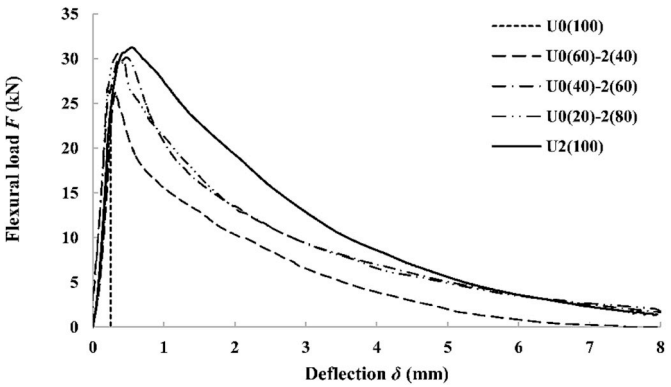

Fig. 9. Flexural load-deflection curve with various bottom layer thickness.

initiated from the bottom layer of the UHPFRC beam, and no debonding was observed. These observations are coincident well with the theoretical analysis in Section 2.3: for $\beta = 0.4$–0.8, the critical debonding loads are higher than the cracking loads, and the crack condition for the bottom layer is satisfied prior to that for the top layer.

The relationship between the first cracking load and the layer thickness are illustrated in Fig. 10. It depicts that the first cracking load is insensitive to the change of β in the given range, corresponding with the findings in Section 2.3 (see Fig. 4 with $\alpha = 0.8$ and 1). The calculated first cracking loads applying Eq. (12) are also compared with the experimental data. A reasonable agreement is achieved between the calculated and the averaged experimental results (with errors smaller than 7%, see Table 5), demonstrating the validity of the proposed formulas.

To depict the effects of the layer thickness more clearly, changes of the peak flexural load F_{max} and the energy E with the layer thickness ratio β are given in Fig. 11. For F_{max}, three stages can be distinguished, i.e. the first stage ($\beta = 0$–0.4) has a relatively slow rate of strength increase; the second stage ($\beta = 0.4$–0.6) exhibits a faster increase; and the third stage ($\beta = 0.6$–1.0) has a slower improvement again. A similar tendency is also observed in Ref. [38], which investigates the normal concrete beam reinforced with engineered cementitious composites. Physically, F_{max} is associated with the aggregate governed bridging and fiber governed bridging mechanisms [38,61]. The significant increase of F_{max} at the transition point from the first stage to the second stage indicates that the bridging mechanism changes from the aggregate governed to the fiber governed one [38]. In other words, for a double-layered UHPFRC beam with $\beta < 0.4$, the fiber-reinforced bottom layer is so thin that the crack-bridging effect provided by the fibers is insufficient, and thus the peak load mainly depends on the bridging of the aggregates; conversely, with the increase of the bottom layer thickness the fiber reinforcements can then effectively restrain the crack propagation, hence leading to the jump of F_{max}.

The flexural energy E, defined geometrically by the area below the flexural load-deflection curve, is also significantly improved due to the application of the bottom UHPFRC layer. With β varying from 0.4 to 0.6 and 0.8, E increases approximately 20, 31 and 32 times in comparison to that of U0(100). And the improvement of E is more prominent within the range of $\beta < 0.6$, while further increasing to 0.8 only provides limited enhancement. To further evaluate the contribution of fibers to the flexural performances, the concept of fiber efficiency eff_f is proposed:

$$eff_f = \frac{E}{m_f} \tag{28}$$

where E is the beam flexural energy, m_f is the mass of the fiber incorporated in the beam, and $m_f = \rho\beta HLbV_f$ with the fiber density

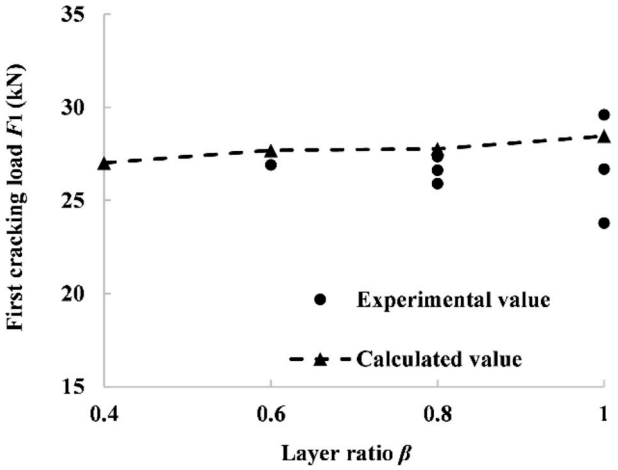

Fig. 10. First cracking strength with various bottom layer thickness.

Table 5
Experimental and calculated first cracking strengths.

Layer thickness ratio β	Averaged first cracking load F_1 (kN)		Error (%)
	Experimental values	Calculated values	
0.4	25.67	27.02	5.3
0.6	26.17	27.68	5.8
0.8	26.63	27.77	4.3
1	26.69	28.46	6.6

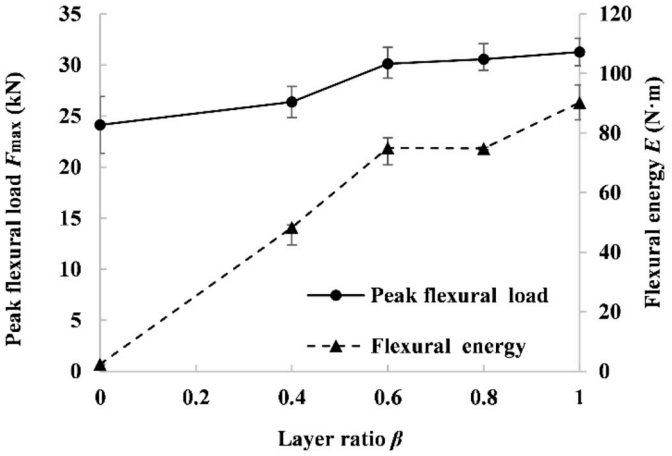

Fig. 11. Peak flexural strength and energy with various bottom layer thickness.

$\rho = 7850\ kg/m^3$. The relation between the fiber efficiency and layer thickness ratio is plotted in Fig. 12, in which the maximum eff_f is reached at $\beta = 0.6$. Consequently, considering the tendency of the first cracking load as well as the improvements of F_{max} and E, $\beta = 0.6$ is selected for the double-layered UHPFRC composite beams and applied in the succeeding analysis.

4.3. Effects of fiber re-arrangement in layered structures

The flexural load-deflection curves of two double-layered UHPFRC beams and a reference single-layered beam are depicted in Fig. 13. The three categories namely U1.2(100), U0(40)-2(60) and U0.6(40)-1.6(60) have an identical total fiber amount, i.e. the equivalent fiber volume fraction is $V_f = 1.2\%$. However, they exhibit distinct flexural capacities due to the fiber re-arrangement in the layered structure. Comparing with

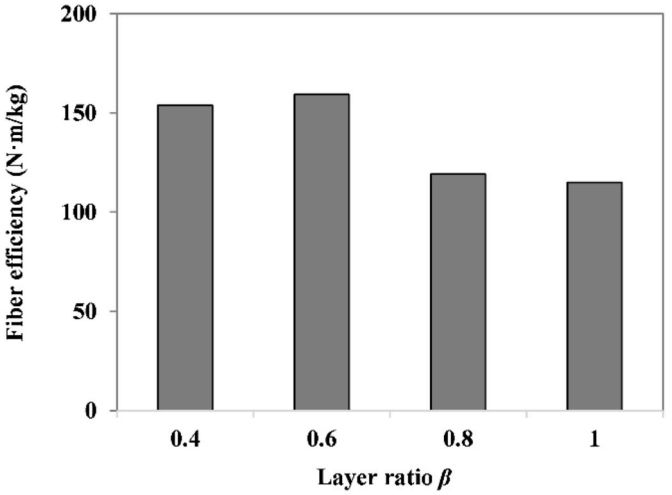

Fig. 12. Fiber efficiency with various bottom layer thickness.

the single-layered UHPFRC beam, the double-layered ones achieve improved peak flexural loads. F_{max} of U0(40)-2(60) and U0.6(40)-1.6(60) are around 30.12 kN and 32.79 kN, which are approximately 14% and 24% higher than that of U1.2(100). In the layered beams, steel fibers are more concentrated at the beam bottom that they efficiently bridge across the lower portion of the crack and delay the opening of the crack upper portion, attributing to the increased load carrying ability of the composite beam.

The fiber re-arrangement also affects the flexural energy E. Due to the lack of steel fibers in the top layer, the post-peak stage of U0(40)-2(60) shows a steeper drop than that of the single-layered beam, which leads to an approximate 10% energy reduction than that of U1.2(100). In contrast, incorporating a small amount of fibers in the top layer generates a superior energy absorption capacity, i.e. E of U0.6(40)-1.6(60) is about 14% higher than that of U1.2(100). On that account, for the purpose of flexural energy enhancement, a small amount of steel fibers is required in the top layer of the UHPFRC composite beam.

It should be noted that the equivalent fiber volume fraction $V_f = 1.2\%$ is taken as an example in this section, but the advantages of applying layered-structure would also be expected when a higher equivalent fiber volume fraction is considered. Furthermore, the higher F_{max} and E of U0.6(40)-1.6(60) also indicate the potential of utilizing a layered beam containing fewer fibers to achieve the same flexural performances as U1.2(100).

The crack propagation is also influenced by the fiber re-arrangement. For the single-layered beam U1.2(100), a single crack is observed during the flexural process, initiating from the middle of the beam bottom and gradually propagating to the beam top surface (Fig. 14). A different cracking process is observed for the double-layered beam U0.6(40)-1.6(60). As illustrated in Fig. 15, the crack first appears at the bottom of U0.6(40)-1.6(60) at around $t = 12$ min after the start of the loading. With the increase of the bending load, the crack opens more widely. At $t = 13.5$ min, a newly-developed small crack appears in the top layer near the layer interface owing to the stress concentration caused by the incompatibility between the layers [53]. The small crack propagates further downwards into the bottom layer as the external load increases, which interrupts the potential layer debonding [62]. At $t = 16.5$ min, the small crack from the interface is connected with the previous crack at the beam bottom, creating a macro-crack. Then this macro-crack further develops upwards, during which fibers at the bottom surface of the beam are gradually pulled out from the matrix. At about $t = 35$ min, fibers near the interface are also pulled out and the failure of the beam is accelerated afterwards.

The comparisons between Figs. 14 and 15 demonstrate that the double-layered UHPFRC beam cracks more slowly than its single-layered counterpart due to the more concentrated fibers at the beam bottom, redistributing the tensile stress and prohibiting the crack initiation. It also takes longer for the double-layered beam to reach the final failure status, i.e. being completely separated into two parts, which is

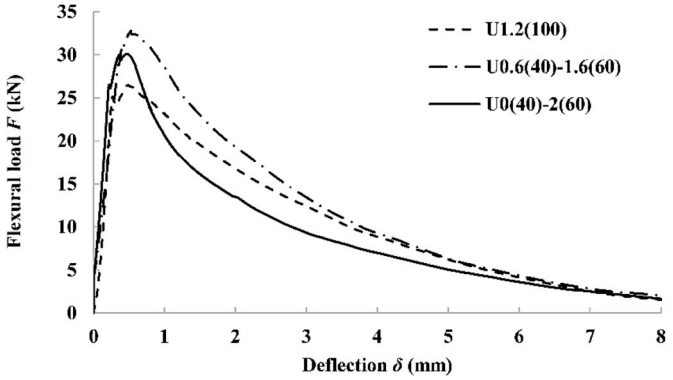

Fig. 13. Flexural load-deflection curve with various fiber re-arrangement.

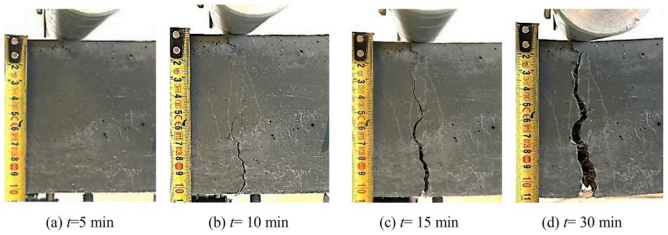

Fig. 14. Crack development in U1.2(100).

attributed to the combined effects provided by the fibers in both the top and the bottom layers. Additionally, the layer interface also serves as a cracking initiator due to the stress concertation and the lack of fiber connection in the interfacial zone. The multiple micro-cracks and fine crack branches in the beam consume more energy during the flexural process and thus improve the flexural energy of the composite beam.

4.4. Effects of fiber content in individual layers

The effects of the fiber content in the individual layers of the UHPFRC composite beam are further evaluated in this section. Figs. 16 and 17 compare the flexural behaviors of U0(40)-1.2(60), U0.6(40)-1.2(60) and U1.2(100). The presented beams have the same fiber content of $V_f = 1.2\%$ in the bottom layer, while V_f in the top layer are 0%, 0.6% and 1.2%, respectively. It is obvious that the compared beams have similar F_{max} although the V_f in their top layers differ, indicating that F_{max} is more related to the fibers in the bottom layer. Nevertheless, improvements of E are observed with an increasing V_f in the top layer, which is associated with the pull-out process of fibers in both the top and the bottom layers. However, the energy enhancement is nonlinear that it is more obvious when top layer V_f increases from 0.6% to 1.2% than from 0% to 0.6%.

On the other hand, changing V_f in the bottom layer generates more prominent effects (see Figs. 18 and 19). Comparing U0(40)-1.2(60) with U0(40)-2(60) reveals that when the top layer is plain concrete, increasing bottom layer V_f from 1.2% to 2% leads to 13% and 16% increase of F_{max} and E, respectively. These improvements become more significant when 0.6% steel fibers are incorporated in the top layer, i.e. U0.6(40)-1.2(60) and U0.6(40)-1.6(60). Namely, 19% and 38% enhancements of F_{max} and E are achieved for these beams when the bottom layer V_f increases from 1.2% to 1.6%.

The above analysis shows the different effects of steel fibers in the individual layers. The enhancement of peak flexural load is more related to the fibers in the bottom layer as they increase the stiffness of the beam, thanks to the bond interaction with the matrix. Fibers in the both layers contribute to the beam flexural energy by connecting the crack surfaces, decelerating the crack development and extending the time for the beam to reach its final failure. Furthermore, considering that the crack width in the upper section of the beam is much narrower than that in the beam bottom, incorporating a small amount of steel fibers in the top layer is sufficient to generate pronounced effects.

5. Conclusions

This paper presents theoretical and experimental investigations on the flexural properties of double-layered UHPFRC with coarse aggregates incorporated and fibers efficiently distributed. Deterministic criteria and formulas for calculating the critical failure load at the first failure stage are developed in the theoretical section, based on which the double-layered beams are designed for the experimental section. Basic mechanical properties as well as the interfacial characteristics of the double-layered UHPFRC are investigated, and three-point bending tests are conducted to study the beam flexural performances. Both the elastic stage and the post-peak behavior are taken into account, providing

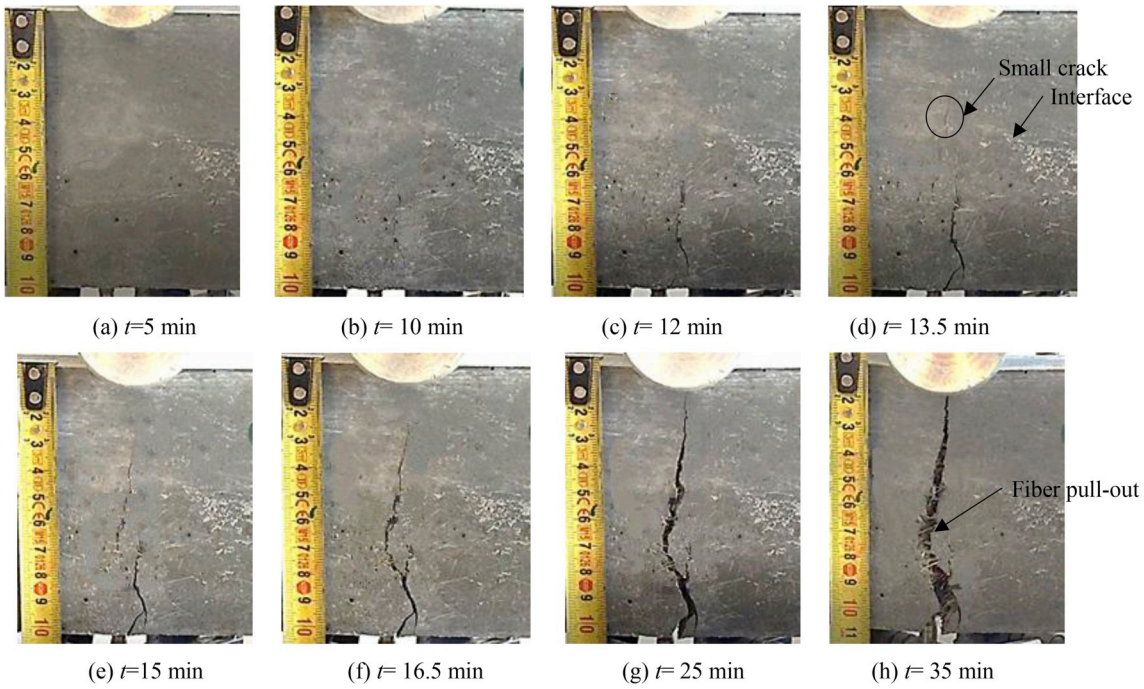

Fig. 15. Crack development in U0.6(40)-1.6(60).

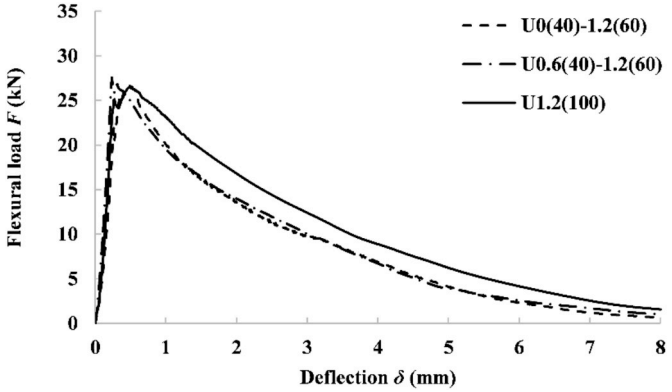

Fig. 16. Flexural load-deflection curve with various fiber contents in top layer.

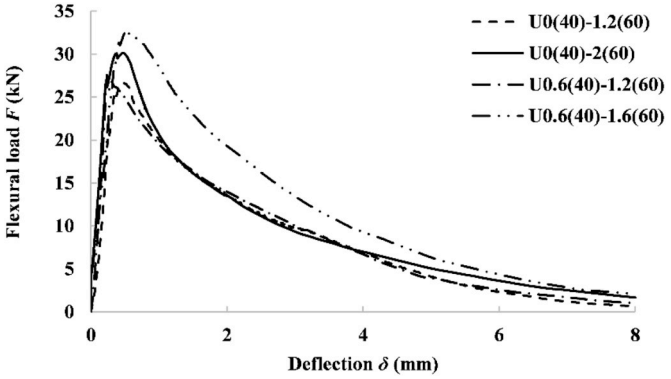

Fig. 18. Flexural load-deflection curve with various fiber contents in bottom layer.

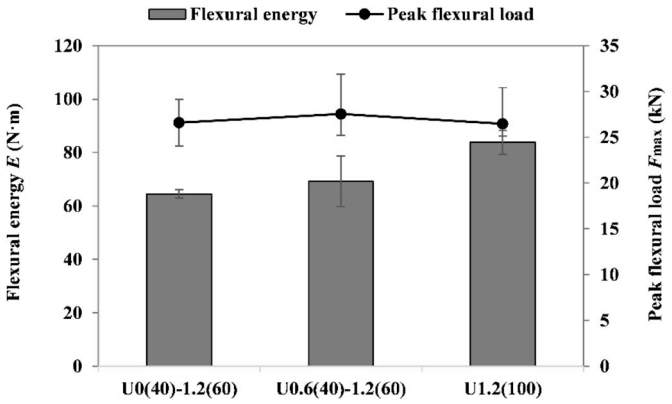

Fig. 17. Effects of fibers in top layer on peak flexural load and flexural energy.

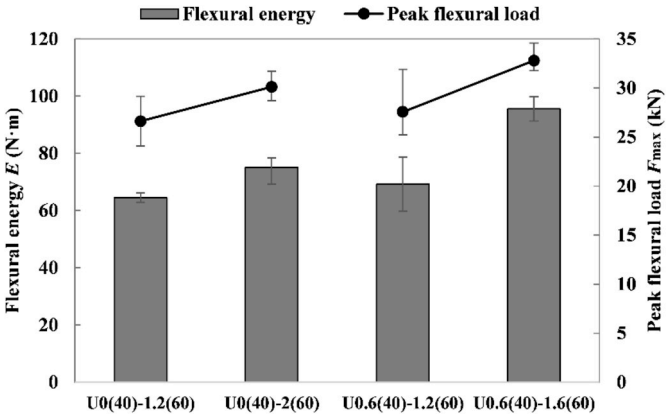

Fig. 19. Effects of fibers in bottom layer on peak flexural load and flexural energy.

valuable information for better designing layered composites. The effects of layer thickness, fiber re-arrangement in the layered structure, as well as the fiber content in the individual layers are discussed, which

sheds light on the enhancement mechanisms in the layered structure. The following conclusions can be drawn from the acquired results:

(1) As confirmed by both the theoretical analysis and the experiment results, the first failure stage of the double-layered beam tends to end with bottom layer cracking rather than layer debonding in most cases (layer thickness ratio $\beta = 0.2$–1.0 with sufficient bond strength, e.g. $\sigma_b = \sigma_{t,1}$).
(2) The peak flexural load F_{max} and the flexural energy E are remarkably improved with the increase of the bottom layer thickness until $\beta = 0.6$ is reached. A jump of F_{max} is observed at $\beta = 0.4$, which is associated with the transition from aggregate governed bridging to fiber governed bridging.
(3) Fiber re-arrangement in the layered structure affects F_{max} and E, as well as the cracking process in the double-layered UHPFRC beam. Compared to the single-layered UHPFRC beam with the same total fiber content, the designed double-layered beam U0.6 (40)-1.6(60) achieves a 24% higher of F_{max} and a 14% higher of E. This also indicates the potential of utilizing layered beams containing fewer fibers to obtain advantageous flexural performances.
(4) Fibers in the bottom layer contribute to the improvement of F_{max} while the increase of E is affected by the fiber content V_f in both layers. A combination of a small V_f in the top layer and a large V_f in the bottom layer can result in the optimal flexural performances with both improved peak flexural load and energy.

This study presents a detailed analysis on the static bending performances of the double-layered UHPFRC, and confirms the advantages of applying layered structure by both theoretical and experimental investigations. Based on this study, layered UHPFRC with an increased layer number and optimal layer thicknesses can be one direction for the further investigations. Moreover, since UHPFRC has a wider military application to resist impacts [63], comprehensive studies of layered UHPFRC exposed to dynamic loads are also of great significance for the further work.

Acknowledgements

This research was carried out under the funding of China Scholarship Council and Eindhoven University of Technology. Furthermore, the authors wish to express their gratitude to the following sponsors of the Building Materials research group at TU Eindhoven: Rijkswaterstaat Grote Projecten en Onderhoud; Graniet-Import Benelux; Kijlstra Betonmortel; Struyk Verwo; Attero; Enci; Rijkswaterstaat Zee en Delta-District Noord; Van Gansewinkel Minerals; BTE; V.d. Bosch Beton; Selor; GMB; Icopal; BN International; Eltomation, Knuaf Gips; Hess AAC Systems; Kronos; Joma; CRH Europe Sustainable Concrete Centre; Cement & Beton Centrum; Heros; Inashco; Keim; Sirius International; Boskalis; NNERGY; Millvision; Sappi and Studio Roex (in chronological order of joining).

References

[1] Hannawi K, Bian H, Prince-Agbodjan W, Raghavan B. Effect of different types of fibers on the microstructure and the mechanical behavior of Ultra-High Performance Fiber-Reinforced Concretes. Compos B Eng 2016;86:214–20. https://doi.org/10.1016/j.compositesb.2015.09.059.
[2] Wu Z, Shi C, He W. Comparative study on flexural properties of ultra-high performance concrete with supplementary cementitious materials under different curing regimes. Constr Build Mater 2017;136:307–13. https://doi.org/10.1016/j.conbuildmat.2017.01.052.
[3] Cao YYY, Yu QL. Effect of inclination angle on hooked end steel fiber pullout behavior in ultra-high performance concrete. Compos Struct 2018;201:151–60. https://doi.org/10.1016/j.compstruct.2018.06.029.
[4] Shi C, Wu Z, Xiao J, Wang D, Huang Z, Fang Z. A review on ultra high performance concrete: Part I. Raw materials and mixture design. Constr Build Mater 2015;101:741–51. https://doi.org/10.1016/j.conbuildmat.2015.10.088.
[5] Yoo DY, Banthia N. Mechanical properties of ultra-high-performance fiber-reinforced concrete: a review. Cement Concr Compos 2016;73:267–80. https://doi.org/10.1016/j.cemconcomp.2016.08.001.
[6] Sobuz HR, Visintin P, Mohamed Ali MS, Singh M, Griffith MC, Sheikh AH. Manufacturing ultra-high performance concrete utilising conventional materials and production methods. Constr Build Mater 2016;111:251–61. https://doi.org/10.1016/j.conbuildmat.2016.02.102.
[7] Shaikh FU, Nishiwaki T, Kwon S. Effect of fly ash on tensile properties of ultra-high performance fiber reinforced cementitious composites (UHP-FRCC). J Sustain Cem Mater 2018;7:357–71. https://doi.org/10.1080/21650373.2018.1514672.
[8] Li PP, Yu QL, Brouwers HJH. Effect of coarse basalt aggregates on the properties of Ultra-high Performance Concrete (UHPC). Constr Build Mater 2018;170:649–59. https://doi.org/10.1016/j.conbuildmat.2018.03.109.
[9] Peng Y, Wu H, Fang Q, Liu JZ, Gong ZM. Impact resistance of basalt aggregated UHP-SFRC/fabric composite panel against small caliber arm. Int J Impact Eng 2016;88:201–13. https://doi.org/10.1016/j.ijimpeng.2015.10.011.
[10] Wille K, Naman AE, Parra-Montesinos GJ. Ultra - high performance concrete with compressive strength exceeding 150 MPa (22ksi) : a simpler way. ACI Mater J 2011;108:46–53. https://doi.org/10.14359/51664215.
[11] Yoo DY, Kim MJ, Kim SW, Park JJ. Development of cost effective ultra-high-performance fiber-reinforced concrete using single and hybrid steel fibers. Constr Build Mater 2017;150:383–94. https://doi.org/10.1016/j.conbuildmat.2017.06.018.
[12] Wu Z, Shi C, He W, Wang D. Static and dynamic compressive properties of ultra-high performance concrete (UHPC) with hybrid steel fiber reinforcements. Cement Concr Compos 2017;79:148–57. https://doi.org/10.1016/j.cemconcomp.2017.02.010.
[13] Liu X, Yan M, Galobardes I, Sikora K. Assessing the potential of functionally graded concrete using fibre reinforced and recycled aggregate concrete. Constr Build Mater 2018;171:793–801. https://doi.org/10.1016/j.conbuildmat.2018.03.202.
[14] Gong C, Ding W, Mosalam KM, Günay S, Soga K. Comparison of the structural behavior of reinforced concrete and steel fiber reinforced concrete tunnel segmental joints. Tunn Undergr Space Technol 2017;68:38–57. https://doi.org/10.1016/j.tust.2017.05.010.
[15] Meng W, Khayat KH. Improving flexural performance of ultra-high-performance concrete by rheology control of suspending mortar. Compos B Eng 2017;117:26–34. https://doi.org/10.1016/j.compositesb.2017.02.019.
[16] Nguyen DL, Ryu GS, Koh KT, Kim DJ. Size and geometry dependent tensile behavior of ultra-high-performance fiber-reinforced concrete. Compos B Eng 2014;58:279–92. https://doi.org/10.1016/j.compositesb.2013.10.072.
[17] Wille K, El-Tawil S, Naaman AE. Properties of strain hardening ultra high performance fiber reinforced concrete (UHP-FRC) under direct tensile loading. Cement Concr Compos 2014;48:53–66. https://doi.org/10.1016/j.cemconcomp.2013.12.015.
[18] Abbas S, Soliman AM, Nehdi ML. Exploring mechanical and durability properties of ultra-high performance concrete incorporating various steel fiber lengths and dosages. Constr Build Mater 2015;75:429–41. https://doi.org/10.1016/j.conbuildmat.2014.11.017.
[19] SpaSojević A. Structural implications of ultra-high performance fibre-reinforced concrete in bridge design. Serbie et: ingénieur civil diplömée de l'Université de Niš; 2008.
[20] Savino V, Lanzoni L, Tarantino AM, Viviani M. Simple and effective models to predict the compressive and tensile strength of HPFRC as the steel fiber content and type changes. Compos B Eng 2018;137:153–62. https://doi.org/10.1016/j.compositesb.2017.11.003.
[21] B N. Compaction des betons: elements de modelisation et caracterisation experimentale. France: LMT, ENS de Cachan; 1997.
[22] Shen B, Hubler M, Paulino GH, Struble LJ. Functionally-graded fiber-reinforced cement composite: processing, microstructure, and properties. Cement Concr Compos 2008;30:663–73. https://doi.org/10.1016/j.cemconcomp.2008.02.002.
[23] YANG J, HAI R, DONG Y, WU K. Effects of the component and fiber gradient distributions on the strength of cement-based composite materials. J Wuhan Univ Technol 2003;18:61–4.
[24] Naghibdehi MG, Naghipour M, Rabiee M. Behaviour of functionally graded reinforced- concrete beams under cyclic loading. Gradjevinar 2015;67:427–39. https://doi.org/10.14256/JCE.1124.2014.
[25] Mastali M, Ghasemi Naghibdehi M, Naghipour M, Rabiee SM. Experimental assessment of functionally graded reinforced concrete (FGRC) slabs under drop weight and projectile impacts. Constr Build Mater 2015;95:296–311. https://doi.org/10.1016/j.conbuildmat.2015.07.153.
[26] Dias CMR, Savastano H, John VM. Exploring the potential of functionally graded materials concept for the development of fiber cement. Constr Build Mater 2010;24:140–6. https://doi.org/10.1016/j.conbuildmat.2008.01.017.
[27] Yigiter H, Aydin S, Yazici H, Yardimci MY. Mechanical performance of low cement reactive powder concrete (LCRPC). Compos B Eng 2012;43:2907–14. https://doi.org/10.1016/j.compositesb.2012.07.042.
[28] Bencardino F, Rizzuti L, Spadea G, Swamy RN. Experimental evaluation of fiber reinforced concrete fracture properties. Compos B Eng 2010;41:17–24. https://doi.org/10.1016/j.compositesb.2009.09.002.
[29] Wu Z, Khayat KH, Shi C. How do fiber shape and matrix composition affect fiber pullout behavior and flexural properties of UHPC? Cement Concr Compos 2018;90:193–201. https://doi.org/10.1016/j.cemconcomp.2018.03.021.
[30] Yoo DY, Kim S, Park GJ, Park JJ, Kim SW. Effects of fiber shape, aspect ratio, and volume fraction on flexural behavior of ultra-high-performance fiber-reinforced cement composites. Compos Struct 2017;174:375–88. https://doi.org/10.1016/j.compstruct.2017.04.069.

[31] Kim DJ, Park SH, Ryu GS, Koh KT. Comparative flexural behavior of hybrid ultra high performance fiber reinforced concrete with different macro fibers. Constr Build Mater 2011;25:4144–55. https://doi.org/10.1016/j.conbuildmat.2011.04.051.
[32] Wu Z, Shi C, He W, Wu L. Effects of steel fiber content and shape on mechanical properties of ultra high performance concrete. Constr Build Mater 2016;103:8–14. https://doi.org/10.1016/j.conbuildmat.2015.11.028.
[33] Kim JHJ, Lim YM, Won JP, Park HG, Lee KM. Shear capacity and failure behavior of DFRCC repaired RC beams at tensile region. Eng Struct 2007;29:121–31. https://doi.org/10.1016/j.engstruct.2006.04.023.
[34] Luković M, Dong H, Šavija B, Schlangen E, Ye G, Breugel K Van. Tailoring strain-hardening cementitious composite repair systems through numerical experimentation. Cement Concr Compos 2014;53:200–13. https://doi.org/10.1016/j.cemconcomp.2014.06.017.
[35] He Y, Zhang X, Hooton RD, Zhang X. Effects of interface roughness and interface adhesion on new-to-old concrete bonding. Constr Build Mater 2017;151:582–90. https://doi.org/10.1016/j.conbuildmat.2017.05.049.
[36] Xu SL, Wang N, Zhang XF. Flexural behavior of plain concrete beams strengthened with ultra high toughness cementitious composites layer. Mater Struct 2012;45:851–9. https://doi.org/10.1617/s11527-011-9803-0.
[37] Hou L, Xu S, Liu H, Chen D. Flexural and interface behaviors of reinforced concrete/ultra-high toughness cementitious composite (RC/UHTCC) beams. J Adv Concr Technol 2015;13:82–93. https://doi.org/10.3151/jact.13.82.
[38] Zhang J, Leung CKY, Cheung YN. Flexural performance of layered ECC-concrete composite beam. Compos Sci Technol 2006;66:1501–12. https://doi.org/10.1016/j.compscitech.2005.11.024.
[39] Zhang J, Wang Z, Ju X, Shi Z. Simulation of flexural performance of layered ECC-concrete composite beam with fracture mechanics model. Eng Fract Mech 2014;131:419–38. https://doi.org/10.1016/j.engfracmech.2014.08.016.
[40] El-Din HKS, Mohamed HA, Khater MAE-H, Ahmed S. Effect of steel fibers on behavior of ultra high performance concrete. In: First Int. Interact. Symp. UHPC, Des Moines, Iowa; 2016. p. 1–10.
[41] Thomas RJ, Sorensen AD. Review of strain rate effects for UHPC in tension. Constr Build Mater 2017;153:846–56. https://doi.org/10.1016/j.conbuildmat.2017.07.168.
[42] Soltani A, Harries KA, Shahrooz BM. Crack opening behavior of concrete reinforced with high strength reinforcing steel. Int J Concr Struct Mater 2013;7:253–64. https://doi.org/10.1007/s40069-013-0054-z.
[43] Nawy EG. Flexural cracking in concrete structures. Transport Res Rec 1991;1301:22–32.
[44] Smarzewski P. Hybrid fibres as shear reinforcement in high-performance concrete beams with and without openings. Appl Sci 2018;8. https://doi.org/10.3390/app8112070.
[45] Zanotti C, Banthia N, Plizzari G. A study of some factors affecting bond in cementitious fiber reinforced repairs. Cement Concr Res 2014;63:117–26. https://doi.org/10.1016/j.cemconres.2014.05.008.
[46] Li PP, Yu QL. Responses and post-impact properties of ultra-high performance fibre reinforced concrete under pendulum impact. Compos Struct 2019;208:806–15. https://doi.org/10.1016/j.compstruct.2018.10.071.
[47] Brouwers HJH, Radix HJ. Self-compacting concrete: theoretical and experimental study. Cement Concr Res 2005;35:2116–36. https://doi.org/10.1016/j.cemconres.2005.06.002.
[48] Yu QL, Spiesz P, Brouwers HJH. Development of cement-based lightweight composites - Part 1: mix design methodology and hardened properties. Cement Concr Compos 2013;44:17–29. https://doi.org/10.1016/j.cemconcomp.2013.03.030.
[49] Quercia G, Hüsken G, Brouwers HJH. Water demand of amorphous nano silica and its impact on the workability of cement paste. Cement Concr Res 2012;42:344–57. https://doi.org/10.1016/j.cemconres.2011.10.008.
[50] Wang X, Wang K, Taylor P, Morcous G. Assessing particle packing based self-consolidating concrete mix design method. Constr Build Mater 2014;70:439–52. https://doi.org/10.1016/j.conbuildmat.2014.08.002.
[51] Li PP, Yu QL, Brouwers HJH. Effect of PCE-type superplasticizer on early-age behaviour of ultra-high performance concrete (UHPC). Constr Build Mater 2017;153:740–50. https://doi.org/10.1016/j.conbuildmat.2017.07.145.
[52] Document ES, Acceptance U, Document P, En DIN, Version STD. Testing fresh concrete — Part 8: self-compacting concrete - slump-flow test. 2007. p. 2–9.
[53] Thai HT, Nguyen TK, Vo TP, Lee J. Analysis of functionally graded sandwich plates using a new first-order shear deformation theory. Eur J Mech A Solid 2014;45:211–25. https://doi.org/10.1016/j.euromechsol.2013.12.008.
[54] Comité Européen de Normalisation. Testing Hardened Concrete - Part 3: Compressive Strength of Test Specimens. 2009. Eur Stand EN 12390–3.
[55] CEN. EN 12390-6:2000 Testing hardened concrete - Part 6: Tensile splitting strength of test specimens, vol. 44; 2000. p. 1–8.
[56] Qian Y, Zhang D, Ueda T. Tensile bond between substrate concrete and normal repairing mortar under freeze – thaw cycles. In: 4th int. Conf. Durab. Concr. Struct. West Lafayette, IN, USA: Purdue University; 2014. p. 385–92.
[57] Corinaldesi V, Nardinocchi A. Mechanical characterization of Engineered Cement-based Composites prepared with hybrid fibres and expansive agent. Compos B Eng 2016;98:389–96. https://doi.org/10.1016/j.compositesb.2016.05.051.
[58] RILEM TC 162-TDF. Recommendations of RILEM TC 162-TDF: test and design methods for steel fibre reinforced concrete: bending test. Mater Struct 2002;35:579–82. https://doi.org/10.1617/14007.
[59] Kim YY, Lee BY, Bang JW, Han BC, Feo L, Cho CG. Flexural performance of reinforced concrete beams strengthened with strain-hardening cementitious composite and high strength reinforcing steel bar. Compos B Eng 2014;56:512–9. https://doi.org/10.1016/j.compositesb.2013.08.069.
[60] Yun H Do. Flexural behavior and crack-damage mitigation of plain concrete beam with a strain-hardening cement composite (SHCC) layer at tensile region. Compos B Eng 2013;45:377–87. https://doi.org/10.1016/j.compositesb.2012.05.053.
[61] Roesler J, Bordelon A, Gaedicke C, Park K, Paulino G. Fracture behavior and properties of functionally graded fiber-reinforced concrete. AIP Conf Proc 2008;973:513–8. https://doi.org/10.1063/1.2896831.
[62] Noshiravani T, Brühwiler E. Analytical model for predicting response and flexure-shear resistance of composite beams combining reinforced ultrahigh performance fiber-reinforced concrete and reinforced concrete. J Struct Eng 2014;140,04014012. https://doi.org/10.1061/(ASCE)ST.1943-541X.0000902.
[63] Yu R. Development of sustainable protective ultra-high performance fibre reinforced concrete (UHPFRC). Eindhoven University of Technology; 2015.